Modal method for classical diffraction by slanted lamellar gratings

Sam Campbell,[1] Lindsay C. Botten,[2] Ross C. McPhedran,[1,*] and C. Martijn de Sterke[1]

[1]*Centre for Ultrohigh bandwidth Devices for Optical Systems (CUDOS), School of Physics, University of Sydney, NSW 2006, Australia*

[2]*CUDOS, Department of Mathematical Sciences, University of Technology, Sydney, NSW 2007, Australia*

**Corresponding author: ross@physics.usyd.edu.au*

Received July 3, 2008; accepted July 20, 2008;
posted July 30, 2008 (Doc. ID 98141); published September 8, 2008

We consider lamellar gratings made of dielectric or lossy materials used in classical diffraction mounts. We show how the modal diffraction formulation may be generalized to deal with slanted lamellar gratings and illustrate the accuracy and versatility of the new method through study of highly slanted gratings in a homogenization limit. We also comment on the completeness of the eigenmode basis and present tests enabling this completeness to be verified numerically. © 2008 Optical Society of America

OCIS codes: 050.0050, 050.1755, 050.6624.

1. INTRODUCTION

Among the many methods that have been devised to treat electromagnetic diffraction by gratings, those based on representation of fields by modal expansions continue to prove of interest and value [1]. Here we are concerned with the properties of modal methods for gratings composed of dielectric and/or metallic materials, and with the exposition of a new modal formulation for lamellar gratings with slanted walls. We call the new method the differential modal method (DMM).

Dielectric and metal gratings with slanted walls are of theoretical and practical interest. Extending the modal method to treat slanted walls may help improve the performance of algorithms that reduce arbitrary 1D gratings to stacks of lamellar gratings. Such algorithms unavoidably introduce sharp discontinuities in the refractive index profile, a serious problem in the study of metallic gratings [2]. More generally the method can be integrated straightforwardly into modal methods formulated for 2D periodic structures. In practice slanted lamellar gratings have application in blazing, and have recently been shown to allow the unidirectional excitation of surface plasmons at normal incidence [3].

Slanted lamellar gratings have previously been treated using the C method, a profile transformation method due to Chandezon *et al.* [4], and the rigorous coupled wave approach (RCWA) [5]. In the C method, slants in the grating are accounted for using a nonorthogonal curvilinear coordinate system, and the grating profile is treated through a tensorial permittivity and magnetic permeability. This simplifies the boundary conditions at the expense of Maxwell's equations becoming tensorial. In its current form [6] the method has wide applicability and has been used extensively for a variety of applications. The RCWA treats arbitrary grating profiles as lamellar grating stacks, and has the disadvantage that each layer in the discretization requires a separate differential equation to be solved.

In this paper we model slanted lamellar gratings as a stack of N individual lamellar gratings whose modes are coupled using a Bloch mode-matching technique. We use a first-order treatment of mode coupling in the parameter δx, which gives the displacement of one layer from the next in the stack, and then take the limit as $N\to\infty$ and $\delta x\to 0$ to obtain an exponential form for the modal propagation equation through the whole stack. Coupling this at the top and bottom of the stack to the plane wave expansions above and below the grating enables the solution of the grating diffraction problem.

The DMM can furnish accurate results up to angles well beyond 89°, whereas the best previous results to our knowledge were based on a modified Chandezon method [7] and were limited to angles not exceeding 64°. This ability to treat gratings with large slant angles enables us to discuss a surprising homogenization result, where the slanted lamellar grating becomes equivalent to a uniform dielectric or lossy layer for which the relative dielectric constant is given by a simple formula. Crucial to the performance of our approach is accurately treating the constituent lamellar layers composing the slanted structure, for which we use the modal method.

The modal formulation for dielectric lamellar gratings is an electromagnetic theory implementation of the familiar Kronig–Penney model from the quantum theory of the solid state, and was developed independently by Botten *et al.* [8] and by Sheng *et al.* [9]. The method is valid for lamellar gratings composed of lossless materials—either dielectrics or idealized metals—and relies on expanding fields in the grating region in terms of a basis of modes, whose completeness was demonstrated by Botten *et al.* [8]. It has the advantage that structures can be accurately

1084-7529/08/102415-12/$15.00

treated independently of their depth [10], and that in some circumstances quite severely truncated modal bases can be used to good accuracy, permitting semianalytic formulas to be derived for diffraction solutions.

The analogy with the Kronig-Penney model becomes less evident for lamellar gratings that include lossy materials, since quantum mechanical wave functions are based on conservation of probability, whereas electromagnetic fields in the presence of loss are nonconservative, losing energy to ohmic dissipation. The resolution of this difficulty put forward by Botten *et al.* [11] was to abandon self-adjoint bases, and to use one basis of modes for expanding functions and an adjoint basis to enforce continuity equations at boundaries between modal and plane-wave expansions by projection. Naturally, as the loss tends to zero, the adjoint basis reduces to the complex conjugate of the field basis, restoring the self-adjoint nature of the lossless solution. Note that the numerical implementation of the modal method in the presence of loss requires the calculation of an accurate and adequately large set of complex solutions of a transcendental equation; one method for doing this is to use a sophisticated algorithm based on complex variable theory [12].

A further development of the modal method in the presence of loss was provided by Roberts aud McPhedran [13]. They showed that the modal basis for a grating composed of dielectric and metallic elements could be divided into two groups, one oscillating slowly in the dielectric and more rapidly in metal (β modes), and the other (γ modes) oscillating more slowly in the metal and rapidly in air. In the infinitely conducting limit, the β modes tend to those expected for fields in dielectric, while the γ modes tend to those used in expanding surface currents in a dual formulation to the beta formulation based on dielectric fields. To achieve accurate solutions for finitely conducting lamellar gratings, both β and γ sets must be adequately populated, and we discuss in Section 2 a convenient numerical test [14] that indicates whether this has been achieved.

Important extensions of the modal method were provided by Li [15,16], who generalized it from the classical diffraction mount to conical diffraction, provided a proof of completeness of the conical modal basis, and showed how to take into account multiple stacked lamellar grating layers. The extensions of the formulation to multiple lamellar elements within a grating period and to a vector Fresnel treatment were carried out by Miller *et al.* [17], Kaushik [18], and Campbell *et al.* [19].

Before treating gratings with slanted walls, we investigate in Section 2 claims regarding the completeness of the lamellar modal formulation when the grating includes materials with real and negative dielectric constants, recently set forth by Sturman *et al.* [20,21]. We first comment on modal method formulations in lossy and lossless systems, before demonstrating that the concerns of Sturman *et al.* were resolved previously by Roberts and McPhedran [13]. After that we generalize the modal formulation to deal with lamellar gratings having slanted walls. In Section 3 we detail this new method for both TE or E_z polarization (incident electric field parallel to the generator of the grating) and for TM or H_z polarization. In Section 4 we verify the accuracy of the DMM by comparing its results with those of Granet *et al.* [22], obtained using the C method [4]. We then study in detail the performance of the method for slanted lamellar gratings, where the slant angle approaches 90°.

2. MODAL DIFFRACTION FORMULATIONS AND COMPLETENESS

Before reporting our extensions to the modal method for slanted diffraction gratings, we address briefly two recent papers by Sturman *et al.* [20,21], who have commented on the choice of optical eigenmodes in metal—dielectric structures. They point out the failure of the analogy with quantum mechanics in this case and comment on the need to use modes whose propagation constants squared are complex even in the case of systems without dissipative loss, in particular in the important case of surface plasmons where the dielectric constant is real and negative: $\epsilon' < 0$, $\epsilon'' = 0$. They comment [21] (p. 1) in relation to this point that:

> Among the literature, we know a couple of papers where the authors mention, on the basis of particular model calculations, that some values of β^2 [23] (Reference is to the note below; it does not pertain to the quoted paper.) cease to be real for $\epsilon'' = 0$. It seems to be that the above warnings remain unknown and/or not understood in the optical community.

To the contrary this case is well understood in the literature as we show below, but first we comment on the formulation of the lamellar diffraction grating model for systems without and with at least one lossy medium. Our discussion will address issues connected with the need to include an adequate set of eigenmodes to ensure accuracy, and numerical tests that can indicate when this is being achieved. Following these comments we will study the limit as $\epsilon'' \to 0$ of the mode-adjoint basis, while evaluating completeness estimates for each set of modes. In particular, we will show that the modes claimed to be "unknown and/or not understood" are in fact just the γ modes studied by Roberts and McPhedran [13].

As we shall see in Section 3, modal formulations rely on the establishment of a complete set of modes $\{u_m(x)v_m(y)\}$, each mode characterized by a propagation constant along the x axis denoted β_m in material 1 and γ_m in material 2. For H_z polarization these constants satisfy the two equations

$$\cos(\beta_m c)\cos(\gamma_m g) - \frac{1}{2}\left(\frac{\beta_m \epsilon_2}{\gamma_m \epsilon_1} + \frac{\gamma_m \epsilon_1}{\beta_m \epsilon_2}\right)\sin(\beta_m c)\sin(\gamma_m g) = \cos(\alpha_0 d), \tag{1}$$

$$\gamma_m^2 = \beta_m^2 + k_0^2(\epsilon_2 - \epsilon_1), \tag{2}$$

where c is the width of material 1 and g is the width of material 2. The modal eigenfunctions satisfy the electromagnetic boundary conditions at interfaces between different materials and obey a quasi-periodicity condition controlled by the quantity α_0:

$$u_m(x+d) = u_m(x)\exp(i\alpha_0 d), \quad \alpha_0 = 2\pi\sin(\phi)/\lambda, \tag{3}$$

for an incident wave of wavelength λ approaching the grating of period d at an angle ϕ to the grating normal. These modes are used to characterize fields in the grating region, while in free space the complete plane-wave basis normalized to the grating period is used to expand fields:

$$w_p^{\pm}(x,y) = \frac{1}{\sqrt{d}}\exp(i\alpha_p x)\exp(\pm i\chi_p y), \tag{4}$$

where the $\pm$ denotes upward and downward propagating states, and where

$$\alpha_p = \alpha_0 + 2\pi p/d, \tag{5}$$

$$\chi_p = \begin{cases} \sqrt{(k_0^2 - \alpha_p^2)} & \text{for } |\alpha_p| \le k_0 \\ i\sqrt{(\alpha_p^2 - k_0^2)} & \text{for } |\alpha_p| > k_0 \end{cases}. \tag{6}$$

Matching the plane wave expansions and the modal expansions at the interfaces between free space and the grating then solves the diffraction problem.

In the case of a lamellar grating composed only of dielectric materials, we can complex conjugate modal functions to obtain an orthogonal set of functions also obeying the appropriate boundary conditions at interfaces, but with a quasi-periodicity condition corresponding to the Bloch factor $\exp(-i\alpha_0 d)$:

$$\overline{u_m(x+d)} = \overline{u_m(x)}\exp(-i\alpha_0 d). \tag{7}$$

It is the fact that the product $u_m(x)\overline{u_l(x)}$ is periodic, together with both functions obeying the same boundary conditions, that leads to their orthogonality:

$$\int_d \overline{u_l(d)}u_m(x)\mathrm{d}x = \delta_{lm}, \tag{8}$$

using the form of the scalar product appropriate for E_z polarization.

The idea of the completeness test proposed in [14] is simple. To test the completeness of a truncated set of modes, we use the modes to expand plane waves, using the inner product between the x-dependent part of the pth plane wave and the lth mode:

$$P_{pl} = \frac{1}{\sqrt{d}}\int_d \exp(-i\alpha_p x)u_l(x)\mathrm{d}x. \tag{9}$$

Then

$$\frac{1}{\sqrt{d}}\exp(i\alpha_p x) = \sum_m \overline{P_{pm}}u_m(x), \tag{10}$$

so that

$$\frac{1}{d}\int_d \exp(i(\alpha_p - \alpha_q)x)\mathrm{d}x = \delta_{pq} = \sum_m \overline{P_{pm}}P_{qm}, \tag{11}$$

or in matrix form

$$\mathbf{P}\mathbf{P}^{\mathrm{H}} = \mathbf{I}. \tag{12}$$

We note that an analogous expression exists for the completeness of the plane wave basis in terms of the modal basis.

The expression in Eq. (11) provides a convenient numerical test of completeness. An appropriate number of plane waves is chosen, and the completeness matrix on the right-hand side of Eq. (11) is filled in for p and q running over the set of plane waves. The maximum deviation from the required value (one or zero) can be used as an estimate of the completeness of the set of modes used, which should be enlarged until an accuracy tolerance is attained. Note that this is in fact shown by experience to be a reliable but stringent test: far-field quantities such as the efficiencies of diffracted orders can converge more quickly than this near-field test.

Let us now consider nondielectric lamellar gratings. We at once encounter the problem that mode conjugation can no longer be used to provide a family of functions orthogonal to those used to expand fields since conjugation turns lossy materials into materials with gain, thereby changing the physical nature of the system. The solution put forward by Botten *et al.* [11] was to construct an adjoint set of modes satisfying the same one-dimensional Helmholtz equation

$$f_m''(x) + [k_0^2\epsilon(x) - \mu_m^2]f_m(x) = 0, \tag{13}$$

and boundary conditions—continuity of f_m and $\partial f_m/\partial x$ at interfaces—but with quasi-periodicity corresponding to $-\alpha_0$ rather than α_0. Together the modes and their adjoints, denoted $u_m^A(x)$, obey the biorthogonality relation

$$\int_d u_n^A(x)u_m(x)\mathrm{d}x = \delta_{nm}, \tag{14}$$

which allows us to introduce an adjoint inner product for nondielectric systems:

$$K_{pl} = \frac{1}{\sqrt{d}}\int_d \exp(i\alpha_p x)u_l^A(x)\mathrm{d}x. \tag{15}$$

The completeness test for gratings with loss is now

$$\delta_{pq} = \sum_m K_{pm}P_{qm}. \tag{16}$$

The equivalent expression for H_z polarization involves replacing P_{pl} by a term incorporating the reciprocal of the complex dielectric permittivity:

$$A_{pl} = \frac{1}{\sqrt{d}}\int_d \frac{\exp(-i\alpha_p x)}{\epsilon(x)}u_l(x)\mathrm{d}x, \tag{17}$$

and then the completeness test is

$$\delta_{pq} = \sum_m K_{pm}A_{qm}. \tag{18}$$

We now consider the question raised by Sturman *et al.* in [20,21] concerning the nature of the spectrum of modes in a case of a lamellar grating whose dielectric constant is real, but positive in one region and negative in the other. The implications of this become clear when the differen-

Table 1. Truncation Order[a] as a Function of ϵ''

	N_{pw}					
ϵ_2''	3	5	7	9	11	13
0.3	22	23	26	26	27	27
⋮						
3.0×10^{-8}	22	23	26	26	27	27

[a]Truncation order of the lamellar mode basis necessary to keep the maximum error in the completeness matrix of Eq. (18) below 10^{-3} as a function of the imaginary part of the dielectric permittivity of the metal. Six different truncation orders of the plane wave basis are shown. Data: period $d=5\lambda/4$; $\epsilon_1=1$; width of air region, $d/5$, $\epsilon_2'=-9.6$; width of metal region, $4d/5$; normal incidence $\phi=0°$; H_z polarization.

tial equations are cast in self-adjoint form: $-[p(x)u']'+q(x)u=\xi r(x)u$, with $p(x)=1$, $q(x)=-k_0^2\epsilon(x)$, and $r(x)=1$ for E_z polarization, and $p(x)=1/\epsilon(x)$, $q(x)=-k_0^2$, and $r(x)=1/\epsilon(x)$ for H_z polarization. In both cases $\xi=-\mu^2$, and the primes denote derivatives with respect to x. However, when $\epsilon(x)$ is of mixed sign over the period, the weight function $r(x)$ for H_z polarization is not strictly positive and so fails to satisfy the key condition of Sturm–Liouville theory that is needed to establish that the eigenvalues $\xi=-\mu^2$ are purely real.

Sturman *et al.* point out that the set of propagating and evanescent modes in such cases is not complete, but requires the addition of what they call "anomalous" modes with complex propagation constants. The results of our first investigation into this question are given in Table 1 (using the parameters from Fig. 1 of [20] and reproduced in the caption of Table 1), where we show the completeness indicator of Eq. (18) for differing numbers of modes as the imaginary part of the dielectric constant in region 2 of the grating, ϵ_2'', tends to zero.

We can see from Table 1 that the basis consisting of modes and their adjoints remains complete as $\epsilon_2''\to0$, with no tendency whatsoever for the required number of modes to increase. This conclusion is not trivial: if we were operating in the long-wavelength limit, the negative real axis of ϵ would correspond to the location of poles, zeros, and essential singularities of response functions [24,25], thus slowing convergence of series expansions for fields.

As shown by Roberts and McPhedran [13], if either ϵ_2 or ϵ_1 has magnitude much larger than the other in Eq. (1), the modes fall into two clearly distinguished families: β modes, which oscillate slowly in material 1 and show rapid exponential decay into material 2 and γ modes, which oscillate slowly in material 2 and decay rapidly into material 1. Modes can oscillate rapidly in both regions, but then they couple only weakly to propagating plane waves and tend to have little importance in scattering problems. In the very-high-contrast limit either class of modes can be used to solve the diffraction problem: using dual formulations based around guided modes in air between perfectly conducting rods, or modes for the currents flowing on the rods. If both classes are present, the basis is then overcomplete [26] for the perfect conductivity case, but to leave either class out would give an undercomplete basis in any finitely conducting case.

In Table 2 we show the behavior of three modes as $\epsilon_2''\to0$, where the μ here is the β of Sturman *et al.* For the first of these, μ/k_0 tends to a real value, indicating a propagating mode, while for the second it tends to an imaginary value, indicating an evanescent mode. The third mode retains its complex value of μ/k_0 even in the limit of a lossless grating, and is therefore classified by Sturman *et al.* as an "anomalous" mode. On the other hand it is a special case of the complex modes well known in the optics community, and indeed is of the type classified by Roberts and McPhedran [13] as a γ mode on the basis of its spatial variation, which is insensitive to the precise value of ϵ_2''.

3. FORMULATION FOR SLANTED GRATINGS

We consider the diffraction of monochromatic plane waves of free-space wavelength λ at an incident angle of ϕ. E_z polarization is considered in Subsections 3.A and 3.B, while the differences with the H_z polarization formulation are detailed in Subsection 3.C.

A. Slanted Lamellar Gratings

The transition we require to make between the modal formulations for conventional and slanted lamellar gratings is illustrated in Figs. 1–3. The strategy builds from the interface between two typical gratings in Fig. 2, takes into account the thickness of each grating, and then takes the limit as the number of gratings in a stack tends to infinity while their thicknesses tend to zero to give a simple expression for the transfer matrix of the slanted grating stack. This may be summarized as follows:

- formulate the transfer matrix for the interface between two offset lamellar gratings $\mathcal{T}_{\text{interface}}$,
- pad the transfer matrix on either side with lamellar diffraction gratings of thickness $\delta y/2$ to give a new transfer matrix $\mathcal{T}_{\text{pad}}=\mathcal{T}_{\text{half-layer}}\mathcal{T}_{\text{interface}}\mathcal{T}_{\text{half-layer}}$,

Table 2. Eigenvalue Behavior as ϵ'' Approaches Zero

	μ/k_0		
ϵ''	Mode 1[a]	Mode 2	Mode 3
1	$1.21731+1.30675\times10^{-2}i$	$1.00074\times10^{-2}+1.49967i$	$9.01411\times10^{-2}-3.86735i$
10^{-2}	$1.21849+1.31871\times10^{-4}i$	$1.00307\times10^{-4}+1.49912i$	$1.20763\times10^{-1}-3.91227i$
10^{-4}	$1.21849+1.31871\times10^{-6}i$	$1.00307\times10^{-6}+1.49912i$	$1.21300\times10^{-1}-3.91282i$
10^{-6}	$1.21849+1.31871\times10^{-8}i$	$1.00307\times10^{-8}+1.49912i$	$1.21305\times10^{-1}-3.91282i$
10^{-8}	$1.21849+1.31871\times10^{-10}i$	$1.00307\times10^{-10}+1.49912i$	$1.21305\times10^{-1}-3.91282i$
10^{-10}	$1.21849+1.31871\times10^{-12}i$	$1.00303\times10^{-12}+1.49912i$	$1.21305\times10^{-1}-3.91282i$

[a]Mode 1 is a propagating mode in the limit as $\epsilon_2''\to0$, mode 2 is an evanescent mode, and mode 3 is an "anomalous" mode. Data as in Table 1.

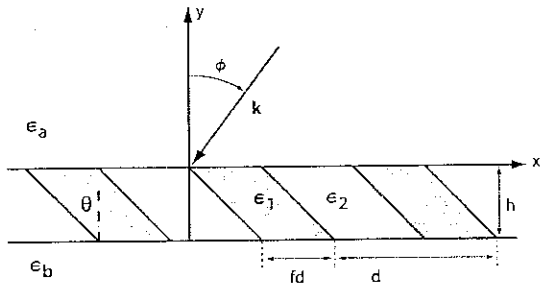

Fig. 1. (Color online) Geometry of the slanted lamellar grating. The subscripted ϵ terms are dielectric constants, θ is the slant angle, ϕ is the incident angle, d is the period, f is the fill fraction, and h is the thickness of the slanted lamellar grating.

- retain terms only to first order in the layer offset δx,
- take the limit as $N=h/\delta y \to \infty$ for $\mathcal{T}_{\text{pad}}^{N}$ to give the transfer matrix for the slanted lamellar grating $\mathcal{T}$.

Here N is the number of padded cells, and h is the total thickness of the slanted lamellar grating.

1. Modal Expansions

The Helmholtz equation Eq. (13) for the modes and the modes-adjoints in a single lamellar grating is treated by separation of variables, with a propagation constant along the y axis for the mth mode being μ_m. Thus, the field component E_z is expanded in modes as

$$E_z = \sum_m \mu_m^{-1/2}[c_m^- \exp(-i\mu_m y) + c_m^+ \exp(i\mu_m y)]u_m(x), \tag{19}$$

while the x component of the magnetic field, rescaled to have the same physical dimension as the electric field, is

$$K_x = \sum_m \frac{1}{k_0}\mu_m^{1/2}[c_m^- \exp(-i\mu_m y) - c_m^+ \exp(i\mu_m y)]u_m(x), \tag{20}$$

where $\vec{K}=\sqrt{\mu_0/\epsilon_0}\vec{H}$.

2. Interface between Displaced Gratings

We wish to treat the interface between two identical lamellar regions, one offset from the other by δx. Denoting region 1 as the layer above and offset by δx from the layer below, region 2, we can write the eigenfunctions in region 1 in terms of the region 2 eigenfunctions:

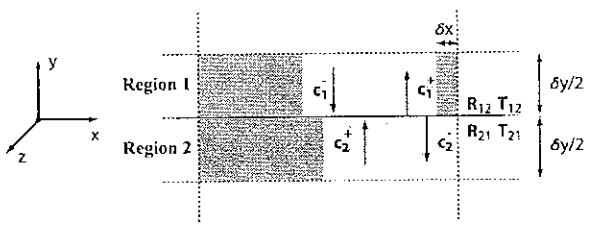

Fig. 2. (Color online) One vertical period of the slanted lamellar grating is shown. Vectors $\mathbf{c}_1^{\pm}$ denote modal amplitudes of basis 1 in region 1, and vectors $\mathbf{c}_2^{\pm}$ denote modal amplitudes of basis 2 in region 2. $\mathbf{R}_{12}$ and $\mathbf{T}_{12}$ denote Fresnel reflection and transmission matrices.

$$u_{1m}(x) = u_{2m}(x - \delta x), \tag{21}$$

$$u_{1m}^A(x) = u_{2m}^A(x - \delta x). \tag{22}$$

To treat the interface between the two lamellar layers we apply the boundary conditions—continuity of E_z and K_x—and use a hybrid projection. Equating the electric fields of Eq. (19) in region 1 and 2 at $y=0$, and projecting onto the adjoint basis by multiplying through by $u_{1l}^A(x)$ and integrating over a period, we find

$$\sum_m \mu_m^{-1/2}(c_{1m}^- + c_{1m}^+)\int_d u_{1m}(x)u_{1l}^A(x)\mathrm{d}x = \sum_m \mu_m^{-1/2}(c_{2m}^- + c_{2m}^+)\int_d u_{2m}(x)u_{1l}^A(x)\mathrm{d}x, \tag{23}$$

or in matrix form

$$\mu^{-1/2}(\mathbf{c}_1^- + \mathbf{c}_1^+) = \mathbf{K}\mu^{-1/2}(\mathbf{c}_2^- + \mathbf{c}_2^+), \tag{24}$$

where $\mu=\mathrm{diag}(\mu_n)$, and

$$K_{lm} = \int_d u_{1l}^A(x)u_{2m}(x)\mathrm{d}x. \tag{25}$$

Note that since the two regions are identical with respect to the eigenvalue equation, the propagation constants μ_m of the two regions are equal.

Applying the boundary condition for K_x leads to

$$\mathbf{J}\mu^{1/2}(\mathbf{c}_1^- - \mathbf{c}_1^+) = \mu^{1/2}(\mathbf{c}_2^- - \mathbf{c}_2^+), \tag{26}$$

where

$$J_{lm} = \int_d u_{2l}^A(x)u_{1m}(x)\mathrm{d}x. \tag{27}$$

Using $u_m^A(\alpha_0,x)=u_m(-\alpha_0,x)$, which states that the adjoint mode becomes the field mode when the sign of the incident angle is flipped, we find

$$\mathbf{J}(\alpha_0) = \mathbf{K}^T(-\alpha_0). \tag{28}$$

To form expressions for the Fresnel matrices $\mathbf{R}_{12}$ and $\mathbf{T}_{12}$ we set $\mathbf{c}_2^+=0$ in Eq. (24) and Eq. (26), then solve for $\mathbf{c}_1^+$ in terms of the incident field $\mathbf{c}_1^-$ for $\mathbf{R}_{12}$ and $\mathbf{c}_2^-$ in terms of $\mathbf{c}_1^-$ for $\mathbf{T}_{12}$. One finds

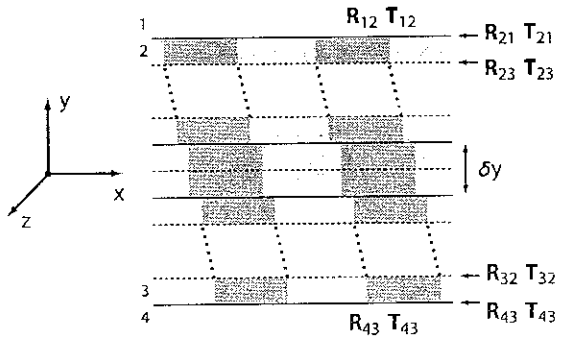

Fig. 3. (Color online) Slanted lamellar grating is formed from a stack of padded cells. The Fresnel matrices $\mathbf{R}_{12}$, $\mathbf{T}_{12}$, $\mathbf{R}_{21}$, and $\mathbf{T}_{21}$ are for the interface between air and a semi-infinite lamellar grating.

$$\mathbf{R}_{12} = (\mathbf{AB} + \mathbf{I})^{-1}(\mathbf{AB} - \mathbf{I}), \tag{29}$$

$$\mathbf{T}_{12} = 2\mathbf{B}(\mathbf{I} + \mathbf{AB})^{-1}, \tag{30}$$

where

$$\mathbf{A} = \boldsymbol{\mu}^{1/2}\mathbf{K}(\alpha_0)\boldsymbol{\mu}^{-1/2}, \tag{31}$$

$$\mathbf{B} = \boldsymbol{\mu}^{-1/2}\mathbf{K}^T(-\alpha_0)\boldsymbol{\mu}^{1/2}. \tag{32}$$

A similar analysis where $c_1^-=0$ leads to expressions for $\mathbf{R}_{21}$ and $\mathbf{T}_{21}$:

$$\mathbf{R}_{21} = (\mathbf{I} + \mathbf{BA})^{-1}(\mathbf{I} - \mathbf{BA}), \tag{33}$$

$$\mathbf{T}_{21} = 2\mathbf{A}(\mathbf{I} + \mathbf{BA})^{-1}. \tag{34}$$

By inspection $\mathbf{A}^T(\alpha_0)=\mathbf{B}(-\alpha_0)$, which leads to the following symmetry properties of the Fresnel matrices:

$$\mathbf{R}_{21}^T(-\alpha_0) = \mathbf{R}_{21}(\alpha_0), \tag{35}$$

$$\mathbf{R}_{12}^T(-\alpha_0) = \mathbf{R}_{12}(\alpha_0), \tag{36}$$

$$\mathbf{T}_{21}^T(-\alpha_0) = \mathbf{T}_{21}(\alpha_0). \tag{37}$$

3. First-Order Expansions in the Layer Shift

In view of taking the limit as the number of layers in a slanted lamellar grating stack approximation goes to infinity, we now derive an expression for $\mathbf{K}$ to first order in δx. To this order Eq. (21) becomes

$$u_{1m}(x) = u_{2m}(x - \delta x), \tag{38}$$

$$= u_{2m}(x) - u'_{2m}(x)\delta x, \tag{39}$$

where the prime denotes a derivative with respect to x. Then Eq. (25) becomes

$$\mathbf{K}(\alpha_0) = \mathbf{I} - \mathbf{V}(\alpha_0)\delta x, \tag{40}$$

where

$$V_{lm} = \int_d \left[\frac{\mathrm{d}}{\mathrm{d}x}u_{2l}(-\alpha_0, x)\right] u_{2m}(\alpha_0, x)\mathrm{d}x. \tag{41}$$

Eq. (31) and Eq. (32) then become

$$\mathbf{A} = \mathbf{I} + \mathbf{M}_A\delta x \qquad \mathbf{M}_A = -\boldsymbol{\mu}^{1/2}\mathbf{V}(\alpha_0)\boldsymbol{\mu}^{-1/2}, \tag{42}$$

$$\mathbf{B} = \mathbf{I} + \mathbf{M}_B\delta x \quad \mathbf{M}_B = -\boldsymbol{\mu}^{-1/2}\mathbf{V}^T(-\alpha_0)\boldsymbol{\mu}^{1/2}. \tag{43}$$

We can now formulate the transfer matrix for an interface to first order in δx:

$$\mathcal{T}_{\text{interface}} = \begin{bmatrix} \mathbf{T}_{12} - \mathbf{R}_{21}\mathbf{T}_{21}^{-1}\mathbf{R}_{12} & \mathbf{R}_{21}\mathbf{T}_{21}^{-1} \\ -\mathbf{T}_{21}^{-1}\mathbf{R}_{12} & \mathbf{T}_{21}^{-1} \end{bmatrix}. \tag{44}$$

After some algebra one finds

$$\mathcal{T}_{\text{interface}} = \mathbf{I} + \begin{bmatrix} \mathbf{M}_a & -\mathbf{M}_s \\ -\mathbf{M}_s & \mathbf{M}_a \end{bmatrix}\delta x + \mathrm{O}(\delta x^2), \tag{45}$$

where

$$\mathbf{M}_s = \tfrac{1}{2}(\mathbf{M}_B + \mathbf{M}_A), \tag{46}$$

$$\mathbf{M}_a = \tfrac{1}{2}(\mathbf{M}_B - \mathbf{M}_A). \tag{47}$$

The padded form of the transfer matrix takes into account propagation through the half-layers above and below the interface (see Fig. 2), and is

$$\mathcal{T}_{\text{pad}} = \begin{bmatrix} \mathbf{Q} & \mathbf{0} \\ \mathbf{0} & \mathbf{Q}^{-1} \end{bmatrix}\left(\mathbf{I} + \begin{bmatrix} \mathbf{M}_a & -\mathbf{M}_s \\ -\mathbf{M}_s & \mathbf{M}_a \end{bmatrix}\delta x\right)\begin{bmatrix} \mathbf{Q} & \mathbf{0} \\ \mathbf{0} & \mathbf{Q}^{-1} \end{bmatrix}, \tag{48}$$

where $\mathbf{Q}=\mathrm{diag}[\exp(i\mu_j\delta y/2)]$. To first order in δy, $\mathbf{Q}=\mathbf{I}+i\boldsymbol{\mu}\delta y/2$, and so retaining terms to first order in δx and $\delta y=\delta x/\tan\theta$, where θ is the slant angle measured from the vertical (see Fig. 2), we find

$$\mathcal{T}_{\text{pad}} = \mathbf{I} + \mathbf{M}\delta y, \tag{49}$$

$$\mathbf{M} = i\begin{bmatrix} \boldsymbol{\mu} & \mathbf{0} \\ \mathbf{0} & -\boldsymbol{\mu} \end{bmatrix} + \tan\theta\begin{bmatrix} \mathbf{M}_a & -\mathbf{M}_s \\ -\mathbf{M}_s & \mathbf{M}_a \end{bmatrix}. \tag{50}$$

4. Limit for an Infinite Number of Grating Layers

We now form the transfer matrix for N layers, where $h=N\delta y$ is the total layer thickness:

$$\mathcal{T}_N = (\mathbf{I} + \mathbf{M}\delta y)^N. \tag{51}$$

In the limit as $N\to\infty$ the transfer matrix for a slanted lamellar grating becomes

$$\mathcal{T} = \lim_{N\to\infty}(\mathbf{I} + \mathbf{M}\delta y)^N = \lim_{N\to\infty}\left(\mathbf{I} + \frac{h}{N}\mathbf{M}\right)^N = \exp(h\mathbf{M}). \tag{52}$$

If $\mathbf{M}$ has the eigensystem decomposition $\mathbf{M}=\mathbf{X}\boldsymbol{\Lambda}\mathbf{X}^{-1}$ then the transfer matrix becomes

$$\mathcal{T} = \mathbf{X}\exp(h\boldsymbol{\Lambda})\mathbf{X}^{-1}. \tag{53}$$

We partition the eigenstates into forward and backward sets: forward states carry energy in the direction of decreasing y for propagating states, decay in the direction of decreasing y for evanescent states, and similarly for the backward states with the direction reversed. For the lossy metallic case all states lose energy because of ohmic dissipation in the direction of their propagation. The matrix $\mathbf{X}$ becomes

$$\mathbf{X} = \begin{bmatrix} \mathbf{F}_- & \mathbf{F}'_- \\ \mathbf{F}_+ & \mathbf{F}'_+ \end{bmatrix}, \tag{54}$$

where the left half of the matrix corresponds to eigenvectors for the forward states with eigenvalues $\exp(h\boldsymbol{\Lambda})$, the right half to the eigenvectors for the backward states with $\exp(-h\boldsymbol{\Lambda}')$. The transfer matrix in Eq. (53) can then be written

$$\mathcal{T} = \begin{bmatrix} \mathbf{F}_- & \mathbf{F}'_- \\ \mathbf{F}_+ & \mathbf{F}'_+ \end{bmatrix}\begin{bmatrix} \exp(h\boldsymbol{\Lambda}) & \mathbf{0} \\ \mathbf{0} & \exp(-h\boldsymbol{\Lambda}') \end{bmatrix}\begin{bmatrix} \mathbf{F}_- & \mathbf{F}'_- \\ \mathbf{F}_+ & \mathbf{F}'_+ \end{bmatrix}^{-1}. \tag{55}$$

Following some algebra

$$\mathcal{T}=\begin{bmatrix}\mathbf{F}_- & \mathbf{F}'_- \\ \mathbf{F}_+ & \mathbf{F}'_+\end{bmatrix}\begin{bmatrix}\exp(h\Lambda) & 0 \\ 0 & \exp(-h\Lambda')\end{bmatrix}\begin{bmatrix}\mathbf{F}^{-1} & 0 \\ 0 & \mathbf{F}'^{-1}_+\end{bmatrix} \times\begin{bmatrix}\mathbf{I} & -\mathbf{R}'_\infty \\ -\mathbf{R}_\infty & \mathbf{I}\end{bmatrix}\begin{bmatrix}(\mathbf{I}-\mathbf{R}'_\infty\mathbf{R}_\infty)^{-1} & 0 \\ 0 & (\mathbf{I}-\mathbf{R}_\infty\mathbf{R}'_\infty)^{-1}\end{bmatrix}, \tag{56}$$

where $\mathbf{R}_\infty=\mathbf{F}_+\mathbf{F}_-^{-1}$ and $\mathbf{R}'_\infty=\mathbf{F}'_-\mathbf{F}'^{-1}_+$. The last give reflection matrices from half-spaces [27] filled with the slanted lamellar grating layers, with incidence in an unslanted structure from above and below the half-spaces

To derive the explicit expressions for the Fresnel matrices $\mathbf{R},\mathbf{T},\mathbf{R}',\mathbf{T}'$ of the slanted lamellar grating we equate Eq. (56) with

$$\mathcal{T}=\begin{bmatrix}\mathbf{T}-\mathbf{R}'\mathbf{T}'^{-1}\mathbf{R} & \mathbf{R}'\mathbf{T}'^{-1} \\ -\mathbf{T}'^{-1}\mathbf{R} & \mathbf{T}'^{-1}\end{bmatrix}, \tag{57}$$

where the primes denote incidence from below. Upon expanding and simplifying we find

$$\mathbf{R}'=(\mathbf{R}'_\infty-\mathbf{P}\mathbf{R}_\infty\mathbf{P}')(\mathbf{I}-\mathbf{R}_\infty\mathbf{P}\mathbf{R}'_\infty\mathbf{P}')^{-1}, \tag{58}$$

$$\mathbf{T}'=(\mathbf{I}-\mathbf{R}_\infty\mathbf{R}'_\infty)\mathbf{P}'(\mathbf{I}-\mathbf{R}_\infty\mathbf{P}\mathbf{R}'_\infty\mathbf{P}')^{-1}, \tag{59}$$

where

$$\mathbf{P}=\mathbf{F}_-\exp(h\Lambda)\mathbf{F}_-^{-1}, \tag{60}$$

$$\mathbf{P}'=\mathbf{F}'_+\exp(h\Lambda')\mathbf{F}'^{-1}_+. \tag{61}$$

For $\mathbf{R},\mathbf{T}$ we note that if upward and downward propagating modes are interchanged ($\Lambda\rightarrow\Lambda'$, $\mathbf{F}'_+\rightarrow\mathbf{F}_-$, $\mathbf{F}'_-\rightarrow\mathbf{F}_+$ and vice versa) then $\mathbf{R}_\infty\rightarrow\mathbf{R}'_\infty$, $\mathbf{R}'_\infty\rightarrow\mathbf{R}_\infty$, $\mathbf{P}\rightarrow\mathbf{P}'$, $\mathbf{P}'\rightarrow\mathbf{P}$, and so

$$\mathbf{R}=(\mathbf{R}_\infty-\mathbf{P}'\mathbf{R}_\infty\mathbf{P})(\mathbf{I}-\mathbf{R}'_\infty\mathbf{P}'\mathbf{R}_\infty\mathbf{P})^{-1}, \tag{62}$$

$$\mathbf{T}=(\mathbf{I}-\mathbf{R}'_\infty\mathbf{R}_\infty)\mathbf{P}(\mathbf{I}-\mathbf{R}'_\infty\mathbf{P}'\mathbf{R}_\infty\mathbf{P})^{-1}. \tag{63}$$

In later sections we will refer to these matrices as

$$\mathbf{R}_{23}=\mathbf{R},$$

$$\mathbf{T}_{23}=\mathbf{T},$$

$$\mathbf{R}_{32}=\mathbf{R}',$$

$$\mathbf{T}_{32}=\mathbf{T}'.$$

B. External Coupling

In the previous subsection the matrices $\mathbf{R}_{23}$, $\mathbf{T}_{23}$, $\mathbf{R}_{32}$, and $\mathbf{T}_{32}$ were calculated, which are the Fresnel matrices for a lamellar modal field incident on a slanted lamellar grating of slope θ and total thickness h. To calculate fields diffracted by the slanted grating we also need the matrices $\mathbf{R}_{12}$, $\mathbf{T}_{12}$, $\mathbf{R}_{21}$, and $\mathbf{T}_{21}$, which are the Fresnel matrices [19,27] between free space and a semi-infinite lamellar grating. The natural choice for expanding the fields above the grating is a plane-wave basis normalized to the grating period:

$$E_z=\sum_p \chi_p^{-1/2}[e_p^-\exp(-i\chi_p y)+e_p^+\exp(i\chi_p y)](1/\sqrt{d})\exp(i\alpha_p x), \tag{64}$$

$$K_x=1/k_0\sum_p \chi_p^{1/2}[-e_p^-\exp(-i\chi_p y)+e_p^+\exp(i\chi_p y)](1/\sqrt{d})\exp(i\alpha_p x), \tag{65}$$

where α_p and χ_p are defined in Eqs. (2)–(4).

Setting Eq. (19) and Eq. (64) equal and projecting onto the plane-wave basis by multiplying through by $\exp(-i\alpha_q x)/\sqrt{d}$ and integrating over a period we have

$$\mathbf{Y}\boldsymbol{\mu}^{-1/2}(\mathbf{c}^-+\mathbf{c}^+)=\boldsymbol{\chi}^{-1/2}(\mathbf{e}^-+\mathbf{e}^+), \tag{66}$$

where

$$\mathbf{Y}_{qm}=\int_d (1/\sqrt{d})\exp(-i\alpha_q x)u_m(x)\mathrm{d}x. \tag{67}$$

Setting Eq. (20) and Eq. (65) equal and projecting onto the adjoint basis by multiplying through by $u_l^A(x)/\sqrt{d}$ and integrating over a period yields

$$\boldsymbol{\mu}^{1/2}(\mathbf{c}^--\mathbf{c}^+)=\mathbf{Z}^T\boldsymbol{\chi}^{1/2}(\mathbf{e}^--\mathbf{e}^+), \tag{68}$$

where

$$\mathbf{Z}_{pm}=\int_d (1/\sqrt{d})\exp(i\alpha_p x)u_m^A(x)\mathrm{d}x. \tag{69}$$

Setting $\mathbf{c}^+=0$ in Eqs. (66) and (68), we find

$$\mathbf{R}_{12}=(\mathbf{GH}+\mathbf{I})^{-1}(\mathbf{GH}-\mathbf{I}), \tag{70}$$

$$\mathbf{T}_{12}=2\mathbf{H}(\mathbf{I}+\mathbf{GH})^{-1}, \tag{71}$$

where

$$\mathbf{G}=\boldsymbol{\chi}^{1/2}\mathbf{Y}\boldsymbol{\mu}^{-1/2}, \tag{72}$$

$$\mathbf{H}=\boldsymbol{\mu}^{-1/2}\mathbf{Z}^T\boldsymbol{\chi}^{1/2}. \tag{73}$$

Setting $\mathbf{e}^-=0$ in Eqs. (66) and (68), we find

$$\mathbf{R}_{21}=(\mathbf{I}+\mathbf{HG})^{-1}(\mathbf{I}-\mathbf{HG}), \tag{74}$$

$$\mathbf{T}_{21}=2\mathbf{G}(\mathbf{I}+\mathbf{HG})^{-1}. \tag{75}$$

We can now write down the Fresnel reflection and transmission matrices for the entire structure by a process of recursion:

$$\mathbf{R}_{14}=\mathbf{R}_{13}+\mathbf{T}_{31}\mathbf{R}_{34}(\mathbf{I}-\mathbf{R}_{31}\mathbf{R}_{34})^{-1}\mathbf{T}_{13}, \tag{76}$$

$$\mathbf{T}_{14}=\mathbf{T}_{34}(\mathbf{I}-\mathbf{R}_{31}\mathbf{R}_{34})^{-1}\mathbf{T}_{13}, \tag{77}$$

where

$$\mathbf{R}_{13}=\mathbf{R}_{12}+\mathbf{T}_{21}\mathbf{R}_{23}(\mathbf{I}-\mathbf{R}_{21}\mathbf{R}_{23})^{-1}\mathbf{T}_{12}, \tag{78}$$

$$\mathbf{T}_{13}=\mathbf{T}_{23}(\mathbf{I}-\mathbf{R}_{21}\mathbf{R}_{23})^{-1}\mathbf{T}_{12}, \tag{79}$$

$$\mathbf{R}_{31}=\mathbf{R}_{32}+\mathbf{T}_{23}\mathbf{R}_{21}(\mathbf{I}-\mathbf{R}_{23}\mathbf{R}_{21})^{-1}\mathbf{T}_{32}, \tag{80}$$

$$\mathbf{T}_{31} = \mathbf{T}_{21}(\mathbf{I} - \mathbf{R}_{23}\mathbf{R}_{21})^{-1}\mathbf{T}_{32}. \tag{81}$$

These enable the solution of the scattering problem for an arbitrary incident plane wave field diffracted by a slanted lamellar grating of arbitrary thickness and slant angle, made either of dielectric materials, lossy materials, or both, for the case of E_z polarization.

C. Differences for the H_z Polarization Case

1. Modal Basis and the Slanted Lamellar Region

Mode integrals for H_z polarization acquire a weight factor equal to the inverse of the dielectric constant:

$$\int_d \frac{1}{\epsilon(x)} u_n^A(x) u_m(x) \mathrm{d}x = \delta_{nm}. \tag{82}$$

The modal expansions in the lamellar grating region are

$$K_z = \sum_m \mu_m^{-1/2}[c_m^- \exp(-i\mu_m y) - c_m^+ \exp(i\mu_m y)]u_m(x), \tag{83}$$

$$E_x = \sum_m \frac{1}{k_0}\mu_m^{1/2}[c_m^- \exp(-i\mu_m y) + c_m^+ \exp(i\beta_m y)]\frac{u_m(x)}{\epsilon(x)}. \tag{84}$$

Equating Eq. (83) in regions 1 and 2 at $y=0$, and projecting onto the adjoint basis by multiplying through by $u_{1l}^A(x)/\epsilon_1(x)$ and integrating over a period, leads to

$$\boldsymbol{\mu}^{-1/2}(\mathbf{c}_1^- - \mathbf{c}_1^+) = \mathbf{K}\boldsymbol{\mu}^{-1/2}(\mathbf{c}_2^- - \mathbf{c}_2^+), \tag{85}$$

where

$$K_{lm} = \int_d \frac{1}{\epsilon_1(x)} u_{1l}^A(x) u_{2m}(x) \mathrm{d}x. \tag{86}$$

Equating Eq. (84) at the interface of regions 1 and 2, and projecting onto the adjoint basis of region 2 $[u_{2n}^A(x)]$,

$$\mathbf{J}\boldsymbol{\mu}^{1/2}(\mathbf{c}_1^- + \mathbf{c}_1^+) = \boldsymbol{\mu}^{1/2}(\mathbf{c}_2^- + \mathbf{c}_2^-), \tag{87}$$

where

$$J_{lm} = \int_d \frac{1}{\epsilon_1(x)} u_{2l}^A(x) u_{1m}(x) \mathrm{d}x. \tag{88}$$

We note that $\mathbf{J}(\alpha_0)=\mathbf{K}^T(-\alpha_0)$. Using this result, and the same approach as in Subsection 3.A.2, we find

$$\mathbf{R}_{12} = (\mathbf{I} + \mathbf{AB})^{-1}(\mathbf{I} - \mathbf{AB}), \tag{89}$$

$$\mathbf{T}_{12} = 2\mathbf{B}(\mathbf{I} + \mathbf{AB})^{-1}, \tag{90}$$

$$\mathbf{R}_{21} = (\mathbf{I} + \mathbf{BA})^{-1}(\mathbf{BA} - \mathbf{I}), \tag{91}$$

$$\mathbf{T}_{21} = 2\mathrm{A}(\mathbf{I} + \mathbf{BA})^{-1}. \tag{92}$$

where **A** and **B** take the same form as in the E_z case, but for a different **K**.

To first order Eq. (21) becomes

$$u_{2m}(x) = u_{1m}(x + \delta x), \tag{93}$$

$$= u_{1m}(x) + u_{1m}'(x)\delta x, \tag{94}$$

and so

$$\mathbf{K}(\alpha_0) = \mathbf{I} + \mathbf{V}(\alpha_0)\delta x, \tag{95}$$

where

$$\mathbf{V}(\alpha_0) = \int_d \frac{1}{\epsilon_1(x)} u_{1l}(-\alpha_0, x)\left[\frac{\mathrm{d}}{\mathrm{d}x} u_{1m}(\alpha_0, x)\right]\mathrm{d}x. \tag{96}$$

Finally

$$\mathcal{T}_{\text{interface}} = \begin{bmatrix} \mathbf{I} + \mathbf{M}_a\delta x & -\mathbf{M}_s\delta x \\ -\mathbf{M}_s\delta x & \mathbf{I} + \mathbf{M}_a\delta x \end{bmatrix}, \tag{97}$$

where now

$$\mathbf{M}_A = \boldsymbol{\mu}^{1/2}\mathbf{V}(\alpha_0)\boldsymbol{\mu}^{-1/2}, \tag{98}$$

$$\mathbf{M}_B = \boldsymbol{\mu}^{-1/2}\mathbf{V}^T(-\alpha_0)\boldsymbol{\mu}^{1/2}, \tag{99}$$

$$\mathbf{M}_a = \tfrac{1}{2}(\mathbf{M}_B - \mathbf{M}_A), \tag{100}$$

$$\mathbf{M}_s = -\tfrac{1}{2}(\mathbf{M}_B + \mathbf{M}_A). \tag{101}$$

From this point the derivation proceeds as for E_z polarization.

2. External Coupling

The field component expansions we now use are

$$K_z = \sum_p \chi_p^{-1/2}[f_p^- \exp(-i\chi_p y) - f_p^+ \exp(i\chi_p y)](1/\sqrt{d})\exp(i\alpha_p x), \tag{102}$$

$$E_x = 1/k_0 \sum_p \chi_p^{1/2}[f_p^- \exp(-i\chi_p y) + f_p^+ \exp(i\chi_p y)] \times (1/\sqrt{d})\exp(i\alpha_p x). \tag{103}$$

Setting Eq. (83) and Eq. (102) equal and projecting onto the adjoint basis of region 1 by multiplying through by $u_{1n}^A(x)/\epsilon_1(x)$ and integrating over a period gives

$$\mathbf{Y}\boldsymbol{\chi}^{-1/2}(\mathbf{f}^- - \mathbf{f}^+) = \boldsymbol{\mu}^{-1/2}(\mathbf{c}^- - \mathbf{c}^+), \tag{104}$$

where

$$Y_{mp} = \int_d (1/\sqrt{d})\exp(i\alpha_p x)[1/\epsilon_1(x)]u_{1m}^A(x)\mathrm{d}x. \tag{105}$$

Setting Eq. (84) and Eq. (103) equal and projecting onto the plane-wave basis gives

$$\boldsymbol{\chi}^{1/2}(\mathbf{f}^- + \mathbf{f}^+) = \mathbf{Z}^T\boldsymbol{\mu}^{1/2}(\mathbf{c}^- + \mathbf{c}^+), \tag{106}$$

where

$$Z_{mq} = \int_d \frac{1}{\sqrt{d}}\frac{1}{\epsilon_1(x)} u_{1m}(x)\exp(-i\alpha_q x)\mathrm{d}x. \tag{107}$$

Note in the E_z polarization case the continuity equation for the electric field is projected onto the plane-wave ba-

sis, whereas the magnetic field continuity equation is projected onto the adjoint modal basis. Here the basis projections are permuted, the required form if the formulation is to have the correct limiting behavior in the infinite conductivity limit as shown by Roberts and McPhedran [13]. The rest of the derivation proceeds as before in the E_z polarization case, with Eqs. (78) and (83) giving the required reflection and transmission matrices.

4. VERIFICATION AND APPLICATIONS

A. Verification

We now establish the accuracy of the new formulation by comparing its results with those from the Chandezon method, taken from Granet *et al.* [22]. The three cases in Table 3 refer to two lossless gratings with (A) low refractive index contrast and (B) high contrast, while (C) corresponds to a good metal.

We see from Table 3 that the agreement between our method and the results of Granet *et al.* is to two significant figures in all cases, with best agreement for E_z polarization. To ensure the accuracy of the results from our method, it is necessary to choose appropriate values for both the number of plane waves M_1 and the number of modes M_2. In doing this we must keep two considerations in mind. First, for a given number of plane waves the number of modes must be sufficient to ensure that the completeness tests described in Section 2 are accurately satisfied (maximum errors of 10^{-6} for E_z, 10^{-5} for H_z). Second, for a given number of modes the number of plane waves must be large enough to avoid *relative convergence* [28,29]. The number of modes and plane waves used in Table 3 corresponds to an absolute accuracy equal to the number of figures quoted. In relation to the method used by Granet *et al.* Li [6] has commented that the Fourier series representations of products of discontinuous functions were not correctly incorporated, which would particularly limit the use of this implementation for large slant angles. Nonetheless, the results of Granet *et al.* quoted here are expected to be of good quality for the small slant angle considered.

In comparing the DMM with other computational methods for diffraction grating scattering, a number of features are clear. First, computational times and accuracy tend to be weak functions of the grating depth. This is not so for other methods, where increasing the profile depth generally leads to slower and less accurate results. Second, the most difficult numerical problems arise in high-contrast gratings for H_z polarization. In the DMM, the choice of modes in this case is critical for the accuracy of results.

When considering metallic gratings we must be careful in choosing the set of grating modes to make sure there is a sufficient number of β and γ modes. In practice all modes that are clearly of the β and γ types, as well as a number of modes that are strongly evanescent in both regions of the lamellar grating must be included.

It should be noted that the DMM starts with a formulation for a lamellar grating with vertical walls and incorporates a slant of those walls as an additional element. It might therefore be expected that the computational accuracy of the method would diminish as the slant angle θ increases. To test this, we study the behavior of both dielectric and metallic slanted lamellar gratings as the

Table 3. Comparison of Efficiencies Calculated Using the DMM and the C Method[a]

		E_z Polarization		H_z Polarization	
Case		C Method	DMM	C Method	DMM
A					
M_1		10	5	10	5
M_2			25	10	25
Reflected orders	−1	0.0179	0.0179	0.023	0.0231
	0	0.0137	0.0137	0.001	0.0011
Transmitted orders	−1	0.0399	0.0398	0.0232	0.0227
	0	0.9286	0.9286	0.9528	0.9531
B					
M_1		40	15	40	15
M_2			75	40	85
Reflected Orders	−1	0.4191	0.4179	0.2742	0.275
	0	0.0562	0.0562	0.2361	0.237
Transmitted orders	−1	0.0232	0.0229	0.096	0.097
	0	0.5015	0.5030	0.3938	0.391
C					
M_1		10	10	20	10
M_2			40		50
Reflected orders	−1	0.2357	0.2359	0.2214	0.2247
	0	0.4269	0.4267	0.3061	0.307
Transmitted orders	−1	0.1645	0.1646	0.2066	0.2075
	0	0.1558	0.1557	0.2408	0.241

[a]For the C method M_1 is the truncation parameter of the Floquet harmonics ($2M_1+1$ in total). For the DMM M_1 is the truncation parameter of plane waves ($2M_1+1$ in total), and M_2 is the truncation parameter for the modal basis. Parameters: $h=0.2$, $f=0.5$, $d=1$, $\theta=10°$, $\lambda=1$, $\phi=30°$, $\epsilon_a=1$, $\epsilon_b=2.1025$ ($n_b=1.45$). Case (A) $\epsilon_1=1$, $\epsilon_2=2.25$ ($n_2=1.5$); (B) $\epsilon_1=1$, $\epsilon_2=25$ ($n_2=5$); (C) $\epsilon=1$, $\epsilon_2=-44.9757+2.9524i$ ($n_2=0.22+i6.71$).

slant angle increases toward 90° in Subsection 4.A below. We note in passing that the original Chandezon method experiences numerical difficulties as the slant angle tends toward zero. Plumey [30] *et al.* and Preist [7] *et al.* extended the Chandezon method to enable it to deal with gratings having a vertical facet, or even overhanging profiles. Preist *et al.* showed that their extended method can cope with slant angles from 0 to 64° for a silver metallic grating, and commented that the method became numerically unstable at high inclination angles because of the greatly increased profile "depth," measured parallel to the originally vertical grating walls, within the period.

For large slant angles, drawing general conclusions for methods whose lineage begins with the original Chandezon method is difficult, as the interaction of theory, numerical algorithms, and programming details would all need to be considered. Nonetheless, one expects this limiting case to present significant challenges to any method, as reported by Preist *et al.* [7], and as experienced in this work, where the truncation order of field expansions must be increased significantly for large slant angles.

B. Large Slant Angles

The difficulty inherent in calculations for lamellar gratings with large slant angles is illustrated in Fig. 4. Here we show the profile of a grating with fill fraction 0.5 and equal height and period. As we increase the slant angle, profile elements from one period begin to intrude into adjacent periods, so that the profile function becomes more and more multivalued. For slant angles approaching 90° the depth of the profile, measured parallel to the originally vertical interfaces, tends to infinity; equally, the number of profiles intersecting a given period also tends to infinity. At the same time as illustrating the computational difficulties associated with extreme slanting, Fig. 4(d) illustrates the possibility of a simple physical outcome: *we might expect that lamellar gratings for slant angles approaching* 90° *become equivalent to alternating thin-film stacks*. Of course for a fixed height the thickness of each layer in the equivalent thin-film stack tends to zero as the number of layers within the stack goes to infinity. Since the layer thickness is becoming a smaller and smaller fraction of the incident light's wavelength we also expect that the stratified thin-film layer could be well approximated by an equivalent layer with an effective or homogenized set of optical properties.

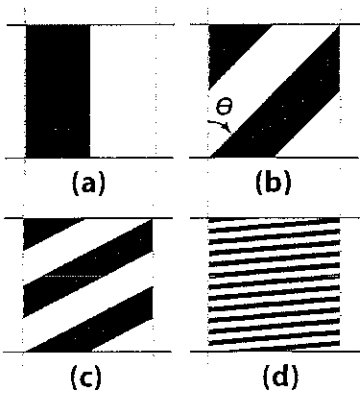

Fig. 4. Schematic periods of slanted lamellar gratings for (a) no slant, (b) $\theta=45°$, (c) $\theta=63.4°$, (d) $\theta=85.2°$.

In Fig. 5 we show the energy reflected from a dielectric lamellar grating for E_z polarization versus slant angle. The oscillations in the reflectance correlate with the variation of the slope angle, as indicated by the vertical lines that mark integer values of $\tan\theta$. Remarkably, the numerical results from the DMM are stable for slope angles as large as 89.99°, which enables us to determine the limiting reflectance for the structure very accurately. In fact at 89.99° the reflectance has converged to four significant figures, and gives the value $R=0.6191$. Referring to Fig. 4(d) we would expect the homogenized dielectric constant of the structure to be the average of the values for air and that for the dielectric regions, i.e., $\epsilon_{\text{eff}}=0.5\times1+0.5\times25=13$. A homogeneous slab with this dielectric constant and the same thickness as the grating gives a reflectance of 0.6191, showing both the accuracy of the homogenization result and the accuracy and stability of the DMM. We also verified that the reflectance versus grating height is predicted to better than graphical accuracy up to at least ten times the period with the same $\epsilon_{\text{eff}}=13$ at $\theta=89.99°$. It follows the phase is correctly reproduced in the E_z homogenized limit, and that the DMM is stable for gratings with large refractive index contrasts, heights, and slant angles.

For H_z polarization and lossless gratings the calculations converge more slowly for large slant angles. Investigations into this numerical problem are in course; however preliminary results indicate the reflectance agrees with the value found for an equivalent dielectric slab where the effective dielectric constant is the average of the gratings' dielectric constants.

We next consider metallic gratings, where perhaps surprisingly both the E_z and H_z polarizations can be addressed with high accuracy up to very large slant angles. In Fig. 6 we show the energy reflected versus slant angle for both polarizations. The characteristic difference between these polarizations is quite evident. For E_z polarization the curve increases smoothly from $R=0.707$ for $\theta=0$ to $R=0.973$ for $\theta=89.99°$. This value agrees again with that expected from a slab with a homogenized dielectric constant obtained from the linear mixing formula: R

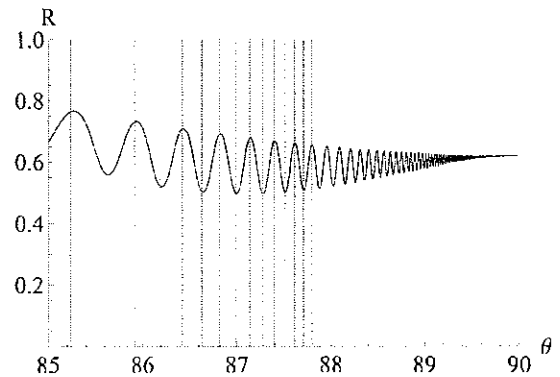

Fig. 5. Energy reflected from a lamellar grating under normal E_z incidence versus slant angle for $f=0.5$, $d=1$, $h=0.5$, $\epsilon_1=1$, $\epsilon_2=25$ ($n_2=5$), $\lambda=1.1$ and the grating suspended in air. Angles where $\tan\theta$ increases by 1 are shown as vertical lines, from $\tan(85.2°)=12$ up to $\tan(87.7°)=26$.

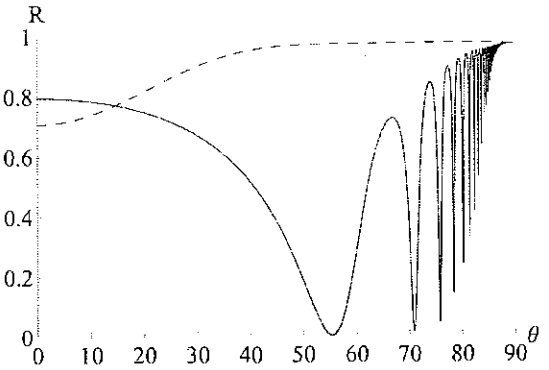

Fig. 6. Energy reflected from a lamellar grating under normal H_z (solid curve) and E_z (dashed curve) incidence versus slant angle θ, with $f=0.5$, $d=1$, $h=0.5$, $\epsilon_1=1$, $\epsilon_2=-44.9757+2.9524i$ ($n_2=0.22+i6.71$), $\lambda=1.1$ and the grating suspended in air.

$=0.973$. For H_z polarization the reflectance is a strongly oscillating function of angle, indicating interference effects. We obtain converged results up to $\theta=89.8°$, and at this angle the reflectance $R=0.972$. Note that for both polarizations the light that is not reflected is absorbed for large slant angles (transmittance of $\sim 10^{-12}$ for E_z, $\sim 10^{-8}$ for H_z).

An important feature of Fig. 6 is that the reflectance is independent of the polarization of the incident wave in the limit of large slant angles. This feature is a consequence of our choice of normal incidence in Fig. 6, and is in keeping with the geometrical limit of Fig. 4. The onset of E_z homogenization is rapid, while the oscillations present in H_z polarization delay the attainment of the limit, and this difference may offer designs with strong polarization dependence.

As our final example we show in Fig. 7 the energy absorbed by the lamellar grating of Fig. 6 for H_z polarization as a function of slant angle and height. Note the interference effects that become increasingly finely spaced as $\theta \to 90°$. The homogenized layer has an absorptance of 0.028, which is much less than the maximum absorptance in Fig. 7. The maximum occurs in a resonance region lying below the homogenized zone; at $h=0.5$, for example, the maximum absorptance is 0.517 and occurs at $\sim\theta = 80°$.

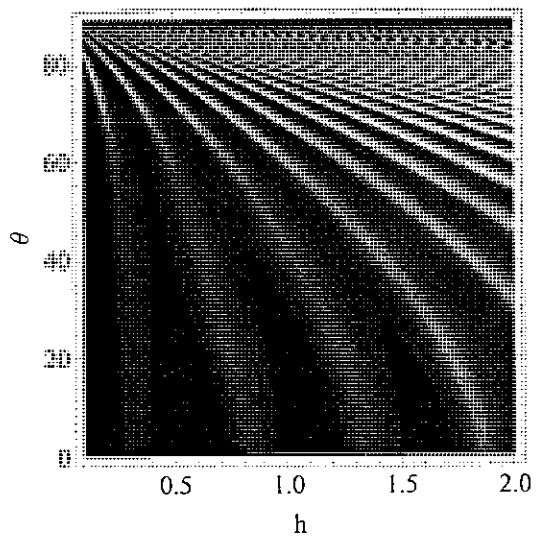

Fig. 7. Energy absorbed by a lamellar grating under normal H_z incidence as a function of slant angle θ and height h, where $f=0.5$, $d=1$, $\epsilon_1=1$, $\epsilon_2=-44.9757+2.9524i$ ($n_2=0.22+i6.71$), $\lambda=1.1$ and the grating suspended in air. The maximum absorptance (lighter fringes) is 0.517, and the minimum is 0.017.

5. DISCUSSION AND CONCLUSIONS

The additions to the modal formulation presented extend the applicability of the method in several interesting ways. Slanted lamellar structures, or combinations of slanted lamellar structures, can now be treated accurately. In fact any grating profile that can be modeled as a stack of lamellar gratings can now be slanted, simply by inclining and offsetting the constituent layers in the stack. This greatly increases the parameter space over which the modal method is applicable. The usefulness of the extensions presented decreases when used for gratings where the inclination angles of the structures' walls are not equal, however. For example in a triangular grating profile one would not necessarily see any improvement if slanted lamellar gratings were used in a lamellar grating stack approximation to the grating.

More possibilities exist in 2D modal formulations, however, where shifts along two orthogonal axes open up a wider range of interesting geometries. For example a 2D grating where the periods are offset in such a way as to produce a helical geometry could be treated. Such a structure has been suggested by Toader and John [31,32] as a three-dimensional photonic crystal that can be fabricated [33], and has previously been discussed in the optical literature on columnar thin films [34].

A more theoretical aspect of the method is the new perspective it offers on homogenization theory. Much of the existing homogenization analysis relies on replicating a structure on an ever smaller scale, or on making the wavelength increase in comparison with the scale size of the structure. Introducing a slanted structure and studying its behavior as the slant angle tends to 90° is a third method, and has the advantages of being carried out at a fixed wavelength and scale size.

To conclude, we have presented extensions to the modal method for lamellar diffraction gratings that now permit the study of slanted structures. We have demonstrated that the new method is accurate and versatile, coping with both dielectric and lossy metallic structures and with slant angles ranging from 0° to very close to 90°. In the latter case we have shown that the grating becomes equivalent to a stratified thin-film structure, and indeed may be replaced by an equivalent, homogenized layer. We hope to pursue applications of the new method in future work, and will also extend it to the case of conical incidence.

ACKNOWLEDGMENTS

This work was produced with the assistance of the Australian Research Council (ARC) discovery grant program, and of the ARC Centres of Excellence program.

REFERENCES AND NOTES

1. M. P. Davidson, "A modal model for diffraction gratings," J. Mod. Opt. **50**, 1817–1834 (2003).
2. E. Popov, M. Neviere, B. Gralak, and G. Tayeb, "Staircase approximation validity for arbitrary-shaped gratings," J. Opt. Soc. Am. A **19**, 33–42 (2002).
3. N. Bonod, E. Popov, L. Li, and B. Chernov, "Unidirectional excitation of surface plasmons by slanted gratings," Opt. Express **15**, 11427–11432 (2007).
4. J. Chandezon, M. T. Dupuis, G. Cornet, and D. Maystre, "Multicoated gratings: a differential formalism applicable in the entire optical region," J. Opt. Soc. Am. **72**, 839–846 (1982).
5. M. G. Moharam and T. K. Gaylord, "Rigorous coupled-wave analysis of planar-grating diffraction," J. Opt. Soc. Am. **71**, 811–818 (1981).
6. L. Li, "Oblique-coordinate system-based Chandezon method for modeling one-dimensional periodic, multilayer, inhomogeneous, anisotropic gratings," J. Opt. Soc. Am. A **16**, 2521–2531 (1999).
7. T. W. Preist, J. B. Harris, N. P. Wanstall, and J. R. Sambles, "Optical response of blazed and overhanging gratings using oblique Chandezon transformations," J. Mod. Opt. **44**, 1073–1080 (1997).
8. L. C. Botten, M. S. Craig, R. C. McPhedran, J. L. Adams, and J. R. Andrewartha, "The dielectric lamellar diffraction grating," Opt. Acta **28**, 413–428 (1981).
9. P. Sheng, R. S. Stepleman, and P. N. Sanda, "Exact eigenfunctions for square wave gratings—application to diffraction and surface-plasmon calculations," Phys. Rev. B **26**, 2907–2916 (1982).
10. J. Y. Suratteau, M. Cadilhac, and R. Petit, "On the numerical study of deep dielectric lamellar gratings," J. Opt. (Paris) **14**, 273–288 (1983).
11. L. C. Botten, M. S. Craig, R. C. McPhedran, J. L. Adams, and J. R. Andrewartha, "The finitely conducting lamellar diffraction grating," Opt. Acta **28**, 1087–1102 (1981).
12. L. C. Botten, M. S. Craig, R. C. McPhedran, and J. L. Adams, "Highly conducting lamellar diffraction gratings," Opt. Acta **28**, 1103–1106 (1981).
13. A. Roberts and R. C. McPhedran, "Power losses in highly conducting lamellar gratings," J. Mod. Opt. **34**, 511–538 (1987).
14. L. C. Botten and R. C. McPhedran, "Completeness and modal expansion methods in diffraction theory," Opt. Acta **32**, 1479–1488 (1985).
15. L. Li, "A modal analysis of lamellar diffraction gratings in conical mountings," J. Mod. Opt. **40**, 553–573 (1993).
16. L. Li, "Multilayer modal method for diffraction gratings of arbitrary profile, depth, and permittivity," J. Opt. Soc. Am. A **16**, 2581–2591 (1993).
17. J. M. Miller, J. Turunen, E. Noponen, A. Vasara, and M. R. Taghizadeh, "Rigorous modal theory for multiply grooved lamellar gratings," Opt. Commun. **111**, 526–535 (1994).
18. S. Kaushik, "Vector Fresnel equations and Airy formula for one-dimensional multilayer and surface relief gratings," J. Opt. Soc. Am. A **14**, 596–609 (1997).
19. S. Campbell, L. C. Botten, C. M. de Sterke, and R. C. McPhedran, "Fresnel formulation for multi-element lamellar diffraction gratings in conical mountings," Waves Random Complex Media **17**, 455–475 (2007).
20. B. Sturman, E. Podivilov, and M. Gorkunov, "Eigenmodes for the problem of extraordinary light transmission through subwavelength holes," EPL **80**, 24002 (2007).
21. B. Sturman, E. Podivilov, and M. Gorkunov, "Eigenmodes for metal-dielectric light-transmitting nanostructures," Phys. Rev. B **76**, 125104 (2007).
22. G. Granet, J. Chandezon, and O. Coudert, "Extension of the C method to nonhomogeneous media: application to nonhomogeneous layers with parallel modulated faces and to inclined lamellar gratings," J. Opt. Soc. Am. A **14**, 1576–1582 (1997).
23. β^2 here is the square of the modes propagation constant, which we denote μ^2.
24. D. J. Bergman, "The dielectric constant of a composite material—A problem in classical physics," Phys. Rep. **43**, 377–407 (1978).
25. G. W. Milton, "Bounds using the analytic method," in *The Theory of Composites* (Cambridge U. Press, 2002), pp. 569–589.
26. L. C. Botten, R. C. McPhedran, and G. W. Milton, "Perfectly Conducting Lamellar Gratings: Babinets Principle and Circuit Models," J. Mod. Opt. **42**, 2453–2473 (1995).
27. L. C. Botten, T. P. White, A. A. Asatryan, T. N. Langtry, C. M. de Sterke, and R. C. McPhedran, "Bloch mode scattering matrix methods for modeling extended PC structures," Phys. Rev. E **70**, 056606 (2004).
28. H. Hoffman, "Relative convergence in mode-matching solutions of mircrostrip problems," Electron. Lett. **10**, 126–127 (1974).
29. T. Itoh and R. Mittra, "Relative convergence phenomenon arising in the solution of diffraction from strip grating on a dielectric slab," Proc. IEEE **59**, 1363–1365 (1971).
30. J. P. Plumey, B. Guizal, and J. Chandezon, "Coordinate transformation method as applied to asymmetric gratings with vertical facets," J. Opt. Soc. Am. A **14**, 610–617 (1997).
31. O. Toader and S. John, "Proposed square spiral microfabrication architecture for large three-dimensional photonic band gap crystals," Science **292**, 1133–1135 (2001).
32. O. Toader and S. John, "Square spiral photonic crystals: Robust architecture for microfabrication of materials with large three-dimensional photonic band gaps," Phys. Rev. E **66**, 016610 (2002).
33. D. Ye, Z. Yang, A. Chang, J. Bur, S. Lin, T. Lu, R. Wang, and S. John, "Experimental realization of a well-controlled 3D silicon spiral photonic crystal," J. Phys. D **40**, 2624–2628 (2007).
34. A. Dirks and H. Leamy, "Columnar microstructure in vapor-deposited thin-films," Thin Solid Films **47**, 219–233 (1977).